Effects of Gravitational Time Dilation in Short-duration Balloon Satellite Flights

Paula Fekete, George Zhang, Johnathon Wilmoth
Department of Physics and Nuclear Engineering, United States Military Academy, West Point, NY 10996, USA
Corresponding author: P. Fekete (email: paula.fekete@westpoint.edu)

Abstract

Chip-Scale Atomic Clocks (CSACs) offer compact, precise timing solutions for dynamic environments, such as high-altitude balloon (HAB) missions. However, their performance under rapid thermal transients, gravitational time dilation (GTD), and mechanical stresses in HABs remains underexplored.

This paper presents both ground-based and in-flight test results from CSACs subjected to simulated and actual HAB conditions. Using Allan deviation analysis, we quantify temperature-induced frequency offsets and demonstrate the feasibility of detecting gravitational time dilation. Across multiple HAB launches, we estimate that the CSACs can detect GTD by measuring cumulative time drift during ascents to altitudes of approximately 30-37 km (100,000-120,000 ft).

Challenges such as CSAC lock loss due to payload swing or thermal fluctuations are examined, informing design recommendations for more robust HAB payloads. We also evaluate CSAC reliability in GPS-denied environments, with implications for military and space applications. The CSACs flown to date were not rated for radiation or magnetic field tolerance. However, the most recent models we acquired, currently untested in flight, were qualified by the manufacturer under military standard (MIL-STD) protocols, including high-g shock and vibration, humidity exposure, magnetic field and voltage sensitivity, electromagnetic interference (EMI), and highly accelerated life testing (HALT). We also discuss performance in the context of these standards.

I. Introduction

Precision timing plays a critical role in modern technological systems that require synchronization under dynamic or constrained conditions, such as global navigation satellite systems (GNSS), secure military communications, and distributed sensor networks. Although traditional atomic clocks offer exceptional stability, their size, weight, and power (SWaP) requirements limit their practicality for mobile or remote operations. Chip-scale atomic clocks have emerged as a compact, low-power alternative, providing comparable short-term stability ($\approx 3.0 \times 10^{-11}$ at $\tau = 1\,\text{hour}$) in a compact form factor [1]. These attributes make CSACs especially valuable for tactical and field-deployed systems in GPS-denied environments, where robust and autonomous timekeeping is essential for navigation, synchronization, and data fusion [2].

High-altitude balloons offer a cost-effective platform for deploying CSACs in near-space conditions. Steerable, long-duration HABs are increasingly prioritized for military surveillance, atmospheric research, and communication relays [3]. GPS remains relatively easy to disrupt or jam, motivating the need for reliable local timing sources. In this context, integrating CSACs aboard HABs could enhance navigation, timing, and data integrity in GPS-denied environments. However, the extreme environmental conditions encountered during HAB flights – rapid thermal cycling (*e.g.*, $-40\,^{\circ}\mathrm{C}$ to $40\,^{\circ}\mathrm{C}$), unpredictable mechanical vibrations, and dynamic pressure changes – pose significant challenges to CSAC performance. Although manufacturers specify nominal operating ranges for CSACs [4], their stability under the transient and harsh conditions of HAB missions remains poorly characterized.

Compounding this issue is the theoretical interplay between gravitational time dilation and atomic clock precision. According to general relativity, clocks at higher altitudes measure time at slightly faster rates than those at the Earth's surface, due to gravitational time dilation [5], [6]. For HABs operating at 30-40 km altitudes, this relativistic effect predicts cumulative time differences on the order of nanoseconds over multi-hour flights [7]. Measuring such deviations with CSACs would not only validate their precision in dynamic environments but also highlight their potential as low-cost instruments for investigating fundamental physics.

Previous studies have focused on CSAC performance in controlled laboratory settings or long-duration space missions [2], [8], leaving a critical gap in understanding their behavior during short-duration HAB flights. Ground-based thermal testing, such as oven-controlled stability trials, provides limited insight into real-world scenarios where temperature fluctuations are abrupt and coupled with mechanical stress. Furthermore, the existing literature lacks practical frameworks for mitigating CSAC lock loss, a phenomenon observed during flight operations where environmental perturbations disrupt atomic coherence, causing the clock's phase to reset [4].

This paper addresses these gaps through a dual approach:

- **Empirical Characterization**: We present results from controlled thermal stability tests ($25\,^{\circ}\mathrm{C}$-$50\,^{\circ}\mathrm{C}$) and multiple HAB flights, analyzing the Allan deviation, phase error, and lock-loss events.
- **Theoretical Modeling**: We evaluate the feasibility of detecting gravitational time dilation using CSACs and assess their potential as standalone timing devices in GPS-denied environments.

Our contributions are threefold:

- **Practical implications**: Identification of CSAC failure modes (*e.g.*, thermal hysteresis, vibration-induced phase drift) and design recommendations for hardening HAB payloads against environmental stressors.
- **Technical insights**: Quantitative analysis of temperature-dependent stability degradation, including a 30% increase in Allan deviation at $50\,^{\circ}\mathrm{C}$).
- **Scientific impact**: Development of an experimental framework for nanosecond-level GTD detection using CSACs aboard HABs, bridging atomic clock metrology with experimental tests of general relativity.

This work directly informs ongoing efforts to deploy CSACs in GPS-denied military systems and paves the way for their use in civilian scientific applications, such as distributed sensor networks and atmospheric research.

II. Theory

A "normal" clock, such as those ranging from wristwatches to grandfather clocks, typically consists of three main components. First, an oscillator, such as a quartz crystal or mechanical gears, generates a stable and cyclical frequency. Second, counters, or a mechanism for tracking and interpreting these oscillations, are needed to convert the cycles into units of time (typically seconds or milliseconds). This may take the form of a gear mechanism or an electronic signal in modern clocks. Finally, the display presents the time in a human-readable format, allowing for easy interpretation and operation.

In a similar manner, atomic clocks provide a stable oscillation cycle through the excitation of atoms via laser and microwave cavities. CSACs specifically use a vertical-cavity surface-emitting laser (VCSEL) heated to $46\,^{\circ}\mathrm{C}$ to tune the transition of cesium atoms. A temperature-controlled quartz crystal oscillator is then continuously compared against the frequency of cesium transitions, providing a radio frequency (RF) output signal that can be read using a CSAC developer board. This output is typically measured using either an oscilloscope to capture the 1 Pulse-Per-Second (1PPS) frequency output or a frequency counter to measure the 1PPS signal or the 10 MHz output signal. In the case of the former, a comparative signal from a separate CSAC or similar signal-producing oscillator is needed to measure the phase difference, *i.e.*, the time-domain difference between the frequencies of the two oscillators.

To evaluate the performance and potential limitations of CSACs aboard high-altitude balloon platforms, it is essential to understand the sources of timing error and the metrics used to characterize clock stability. Timing errors can arise from both intrinsic and environmental factors. Intrinsically, all clocks experience aging, an irreversible drift in frequency over time, as well as short-term fluctuations in stability that are typically characterized using the Allan deviation. Externally, disturbances such as temperature fluctuations, mechanical vibrations, and electromagnetic interference can degrade clock performance. For example, operating outside the manufacturer-specified temperature range may compromise temperature control in the quartz crystal oscillator or increase the rate of spurious hyperfine transitions in the cesium vapor cell. Similarly, exposure to strong magnetic fields or high accelerations during balloon ascent can perturb the frequency output.

Beyond these practical considerations, relativistic effects also contribute to timekeeping error in high-altitude environments. In particular, gravitational time dilation, as predicted by general relativity, causes clocks to tick at different rates depending on their altitude. To quantify this effect for HAB-borne CSACs, we now derive an expression for GTD experienced by a clock rising through the atmosphere over the course of a balloon flight.

A. Starting With the Schwarzschild Metric

To estimate the gravitational time dilation experienced by a CSAC abroad a rising HAB, we begin by considering the spacetime geometry around the Earth. While the Earth is not a perfect sphere, and it rotates, for many practical purposes – including weak-field calculations at altitudes up to 40 km – it is sufficient to approximate the gravitational field as that of a static, spherically symmetric mass. This allows us to model the spacetime using the Schwarzschild metric, which describes the external geometry around a non-rotating, spherically symmetric mass in general relativity [5], [6]. In spherical polar coordinates (t, r, θ, ϕ) the Schwarzschild line element is given by

$$\mathrm{d}s^2 = -\left(1 - \frac{2GM}{c^2 r}\right) c^2\, \mathrm{d}t^2 + \left(1 - \frac{2GM}{c^2 r}\right)^{-1} \mathrm{d}r^2 + r^2 \left(\mathrm{d}\theta^2 + \sin^2\theta\ \mathrm{d}\phi^2\right), \tag{1}$$

where G is the gravitational constant, M is the mass of the gravitated body (in our case, Earth), and c is the speed of light. We now introduce the Schwarzschild radius, a key quantity in general relativity defined as

$$R_{\mathrm{S}} = \frac{2GM}{c^2}. \tag{2}$$

The Schwarzschild radius is not the physical radius of the Earth, but a theoretical length scale that characterizes the curvature of spacetime caused by the mass M. For Earth, this value is approximately $R_{\mathrm{S}} = 8.9$ mm, which is much smaller than the actual Earth radius and confirms that we are working well within the weak-field limit. Substituting R_{S} from Equation 2 into Equation 1 the metric becomes

$$\mathrm{d}s^2 = -c^2\,\mathrm{d}\tau^2 = -\left(1 - \frac{R_{\mathrm{S}}}{r}\right) c^2\,\mathrm{d}t^2 + \left(1 - \frac{R_{\mathrm{S}}}{r}\right)^{-1} \mathrm{d}r^2 + r^2\left(\mathrm{d}\theta^2 + \sin^2\theta\;\mathrm{d}\phi^2\right). \tag{3}$$

In Equation 3

- $\mathrm{d}t$ represents the coordinate time measured by a distant observer (far from the gravitated body),
- $\mathrm{d}\tau$ is the proper time experienced by a clock located at radius r,
- and $\mathrm{d}s^2 = -c^2\,\mathrm{d}\tau^2$ for a clock at rest in the gravitational field.

For applications near the Earth's surface, we denote

- $R = 6.371 \times 10^6$ m, the radius of the Earth, and
- h as the altitude above the surface, so that the total radial coordinate is $r = R + h$.

It is common to express the Schwarzschild metric in terms of square roots

$$\mathrm{d}s^2 = -c^2\,\mathrm{d}\tau^2 = -\left(\sqrt{1 - \frac{R_{\mathrm{S}}}{r}}\; c\;\mathrm{d}t\right)^2 + \left(\frac{\mathrm{d}r}{\sqrt{1 - \frac{R_{\mathrm{S}}}{r}}}\right)^2 + r^2\left(\mathrm{d}\theta^2 + \sin^2\theta\;\mathrm{d}\phi^2\right). \tag{4}$$

B. Expanded Metric After Taylor Expansion

Because the Schwarzschild radius R_{S} is much smaller than the radial distance r for typical balloon launches near the Earth, we can simplify the metric by Taylor expanding the square roots in Equation 4 to first order in $\frac{R_{\mathrm{S}}}{r}$

$$\sqrt{1 - \frac{R_{\mathrm{S}}}{r}} \approx 1 - \frac{R_{\mathrm{S}}}{2r}, \qquad \text{and} \qquad \frac{1}{\sqrt{1 - \frac{R_{\mathrm{S}}}{r}}} \approx 1 + \frac{R_{\mathrm{S}}}{2r}. \tag{5}$$

Substituting the results of Equation 5 into the metric Equation 4, we obtain a more explicit expression that reveals how proper time varies with radial and angular motion

$$\mathrm{d}s^2 = -c^2\,\mathrm{d}\tau^2 = -\left(1 - \frac{R_{\mathrm{S}}}{2r}\right)^2 c^2\,\mathrm{d}t^2 + \left(1 + \frac{R_{\mathrm{S}}}{2r}\right)^2 \mathrm{d}r^2 + r^2\left(\mathrm{d}\theta^2 + \sin^2\theta\;\mathrm{d}\phi^2\right). \tag{6}$$

To simplify the metric for our specific case of a high-altitude balloon rising through the atmosphere, we can consider the symmetry of the Earth's gravitational field. If we align Earth's axis of rotation with the z-axis – a standard assumption that does not reduce the generality of the result – we can treat the motion of the balloon as primarily radial, with negligible motion in the polar direction. This allows us to set $\mathrm{d}\theta = 0$, as the payload does not move in latitude during its ascent. The metric in Equation 6 then simplifies to

$$\mathrm{d}s^2 = -c^2\,\mathrm{d}\tau^2 = -\left(1 - \frac{R_{\mathrm{S}}}{2r}\right)^2 c^2\,\mathrm{d}t^2 + \left(1 + \frac{R_{\mathrm{S}}}{2r}\right)^2 \mathrm{d}r^2 + r^2\sin^2\theta\;\mathrm{d}\phi^2\,. \tag{7}$$

This reduced form highlights the dependence of time dilation on radial motion and, potentially, rotational motion in the ϕ direction. For a purely vertical ascent (no azimuthal motion) the $\mathrm{d}\phi$ term would also drop out – a simplification we can adopt shortly when analyzing the trajectory of the balloon. To better understand the behavior of moving clocks in the gravitational field, we divide both sides of Equation 7 by $-c^2\,\mathrm{d}t^2$

$$\left(\frac{\mathrm{d}\tau}{\mathrm{d}t}\right)^2 = \left(1 - \frac{R_{\mathrm{S}}}{2r}\right)^2 - \left(1 + \frac{R_{\mathrm{S}}}{2r}\right)^2 \left(\frac{1}{c}\frac{\mathrm{d}r}{\mathrm{d}t}\right)^2 - \left(\frac{r}{c}\frac{\mathrm{d}\phi}{\mathrm{d}t}\right)^2 \sin^2\theta. \tag{8}$$

This isolates the squared time dilation factor $\left(\frac{\mathrm{d}\tau}{\mathrm{d}t}\right)^2$, which quantifies how proper time accumulates relative to coordinate time for a clock moving radially and azimuthally in the Schwarzschild geometry.

C. Neglecting the Special Relativity Term

The final term in Equation 8 corresponds to special relativistic time dilation for a clock moving at speed

$$v = r\frac{\mathrm{d}\phi}{\mathrm{d}t}, \tag{9}$$

relative to observers at infinity. Such motion may arise either from Earth's sidereal rotation or from orbital motion (such as in the case of satellites). To estimate the size of this effect for our case, assume the clock is fixed to a payload in a HAB that passively rotates with Earth at the average sidereal sidereal rate of ($T = 23\ \mathrm{h}\ \ 56\ \mathrm{min}\ 4.0905\ \mathrm{s}$). This gives an angular velocity of

$$\omega = \frac{\mathrm{d}\phi}{\mathrm{d}t} = \frac{2\pi}{T} = \frac{2\pi\,\mathrm{rad}}{(23\cdot 3600 + 56\cdot 60 + 4.0905)\ \mathrm{s}} \approx 7.3\times 10^{-5}\,\frac{\mathrm{rad}}{\mathrm{s}}. \tag{10}$$

To compute the special relativistic correction near the surface of Earth, we take the latitude of West Point, NY to be

$$\lambda = 41.3915^\circ, \quad \theta = 90^\circ - \lambda = 48.6085^\circ. \tag{11}$$

The special relativistic time dilation term at Earth's surface $r = R$ at West Point, NY is

$$\left(\frac{R\omega}{c}\right)^2 \sin^2\theta \approx 1.4\times 10^{-12}. \tag{12}$$

At a typical HAB altitude of $h = 3\times 10^4\,\mathrm{m}$, or 30 km, above the surface of Earth's geoid, this becomes

$$\left(\frac{(R+h)\omega}{c}\right)^2 \sin^2\theta \approx 2.4\times 10^{-12}. \tag{13}$$

Although this increases slightly with altitude, both values remain on the order of 10^{-12}. This is three orders of magnitude smaller than what our CSACs can detect, namely, time differences on the order of nanoseconds ($10^{-9}\,\mathrm{s}$). Therefore, for the purpose of our experiment, the special relativistic effects are negligible compared to gravitational time dilation.

We can thus safely drop the special relativistic term from Equation 8, yielding a simplified expression

$$\left(\frac{\mathrm{d}\tau}{\mathrm{d}t}\right)^2 = \left(1 - \frac{R_\mathrm{S}}{2r}\right)^2 - \left(1 + \frac{R_\mathrm{S}}{2r}\right)^2 \left(\frac{1}{c}\frac{\mathrm{d}r}{\mathrm{d}t}\right)^2. \tag{14}$$

This simplified metric isolates the two dominant contributions: gravitational time dilation and any time dilation due to vertical (radial) motion. Similar approximations were adopted in the gravitational time dilation studies of [5], [6], which focused on stationary clocks near the Earth's surface.

D. Gravitational Time Dilation Formula for Clocks Launched in HAB Payloads

We return to the full expression for the derivative of proper time from Equation 8, which accounts for gravitational time dilation, vertical motion, and special relativistic effects due to motion

$$\left(\frac{\mathrm{d}\tau}{\mathrm{d}t}\right)^2 = \left(1 - \frac{R_\mathrm{S}}{2r}\right)^2 - \left(1 + \frac{R_\mathrm{S}}{2r}\right)^2 \left(\frac{1}{c}\frac{\mathrm{d}r}{\mathrm{d}t}\right)^2 - \left(\frac{r}{c}\frac{\mathrm{d}\phi}{\mathrm{d}t}\right)^2 \sin^2\theta. \tag{15}$$

We now assume that the clock is located at an altitude h above Earth's surface, so that $r = R + h$, where R is Earth's radius. Since R is constant, we have $\mathrm{d}r = \mathrm{d}h$. In addition, we identify $\Omega = \frac{\mathrm{d}\phi}{\mathrm{d}t}$, numerically calculated in Equation 10, as the constant angular speed of Earth's sidereal rotation. Using these notations, Equation 15 becomes

$$\left(\frac{\mathrm{d}\tau}{\mathrm{d}t}\right)^2 = \left(1 - \frac{R_\mathrm{S}}{2(R+h)}\right)^2 - \left(1 + \frac{R_\mathrm{S}}{2(R+h)}\right)^2 \left(\frac{1}{c}\frac{\mathrm{d}h}{\mathrm{d}t}\right)^2 - \left(\frac{R+h}{c}\Omega\right)^2 \sin^2\theta. \tag{16}$$

We now rewrite three of the terms in Equation 16 in a form that expresses the altitude h as a small correction to Earth's radius R. This will allow us to perform a Taylor expansion in the small, dimensionless quantity $\frac{h}{R}$, which is typically much less than 1 for HABs

$$1-\frac{R_{\mathrm{S}}}{2(R+h)}=1-\frac{R_{\mathrm{S}}}{2R\left(1+\frac{h}{R}\right)}, \tag{17}$$

$$1+\frac{R_{\mathrm{S}}}{2(R+h)}=1+\frac{R_{\mathrm{S}}}{2R\left(1+\frac{h}{R}\right)}, \tag{18}$$

$$\left(\frac{R+h}{c}\Omega\right)^2=\left(\frac{R}{c}\Omega\right)^2\left(1+\frac{h}{R}\right)^2. \tag{19}$$

No approximations were taken so far. Substituting these results, leads to the full expression for $\left(\frac{\mathrm{d}\tau}{\mathrm{d}t}\right)^2$ in terms of $\frac{h}{R}$ in Equation 16

$$\left(\frac{\mathrm{d}\tau}{\mathrm{d}t}\right)^2=\left(1-\frac{R_{\mathrm{S}}}{2R\left(1+\frac{h}{R}\right)}\right)^2-\left(1+\frac{R_{\mathrm{S}}}{2R\left(1+\frac{h}{R}\right)}\right)^2\left(\frac{1}{c}\frac{\mathrm{d}h}{\mathrm{d}t}\right)^2-\left(\frac{R}{c}\Omega\right)^2\left(1+\frac{h}{R}\right)^2\sin^2\theta. \tag{20}$$

To simplify further, we expand the first two squared terms in Equation 20 using a Taylor approximation in the small quantity $\frac{h}{R}\ll 1$, keeping terms up to first order

$$\left(1-\frac{R_{\mathrm{S}}}{2R}\left(1-\frac{h}{R}\right)\right)^2=1-2\cdot\frac{R_{\mathrm{S}}}{2R}\left(1-\frac{h}{R}\right)+\left(\frac{R_{\mathrm{S}}}{2R}\left(1-\frac{h}{R}\right)\right)^2, \text{ and} \tag{21}$$

$$\left(1+\frac{R_{\mathrm{S}}}{2R}\left(1-\frac{h}{R}\right)\right)^2=1+2\cdot\frac{R_{\mathrm{S}}}{2R}\left(1-\frac{h}{R}\right)+\left(\frac{R_{\mathrm{S}}}{2R}\left(1-\frac{h}{R}\right)\right)^2. \tag{22}$$

The last terms in the two equations above are quadratic in $\frac{R_{\mathrm{S}}}{R}\sim 10^{-9}$, making them of order $\sim 10^{-19}$, or smaller. Consequently, they are negligible in our experiments. Substituting these approximations into Equation 20, we obtain the simplified expression

$$\left(\frac{\mathrm{d}\tau}{\mathrm{d}t}\right)^2=1-\left(\frac{R_{\mathrm{S}}}{R}-\frac{R_{\mathrm{S}}h}{R^2}\right)-\left[1+\left(\frac{R_{\mathrm{S}}}{R}-\frac{R_{\mathrm{S}}h}{R^2}\right)\right]\left(\frac{1}{c}\frac{\mathrm{d}h}{\mathrm{d}t}\right)^2-\left(\frac{R}{c}\Omega\right)^2\left(1+\frac{h}{R}\right)^2\sin^2\theta. \tag{23}$$

Distribute (*i.e.*, expand) all the terms in Equation 23 to obtain

$$\left(\frac{\mathrm{d}\tau}{\mathrm{d}t}\right)^2=1-\frac{R_{\mathrm{S}}}{R}+\frac{R_{\mathrm{S}}h}{R^2}-\left(\frac{1}{c}\frac{\mathrm{d}h}{\mathrm{d}t}\right)^2-\frac{R_{\mathrm{S}}}{Rc^2}\left(\frac{\mathrm{d}h}{\mathrm{d}t}\right)^2+\frac{R_{\mathrm{S}}h}{R^2c^2}\left(\frac{\mathrm{d}h}{\mathrm{d}t}\right)^2-\left(\frac{R\Omega\sin\theta}{c}\right)^2-\left(\frac{h\Omega\sin\theta}{c}\right)^2. \tag{24}$$

To simplify further, we now examine the relative size of each term entering Equation 24. The following small parameters appear in the expression: $\frac{R_{\mathrm{S}}}{Rc^2}\sim 1.6\times 10^{-26}$, and $\frac{R_{\mathrm{S}}h}{R^2c^2}\sim 7.3\times 10^{-29}$, which are many orders of magnitude smaller than the other terms in the expression and can therefore be neglected. This leaves only terms larger than $\sim 10^{-17}$, corresponding to leading-order contributions from gravitational time dilation, vertical motion, and rotational motion. Keeping only the dominant terms in Equation 24, we arrive at a simplified expression

$$\left(\frac{\mathrm{d}\tau}{\mathrm{d}t}\right)^2=1-\left(\frac{R_{\mathrm{S}}}{R}-\frac{R_{\mathrm{S}}h}{R^2}\right)-\left(\frac{1}{c}\frac{\mathrm{d}h}{\mathrm{d}t}\right)^2-\left(\frac{R}{c}\,\Omega\right)^2\left(1+\frac{h}{R}\right)^2\sin^2\theta. \tag{25}$$

This result captures the main relativistic effects to first order in $\frac{h}{R}$, while discarding subdominant corrections that fall well below measurable thresholds. Note that the rotational contribution retains its full quadratic structure in $\left(1+\frac{h}{R}\right)^2$, as it multiplies a large factor $(R\Omega)^2$, making the height-dependent correction potentially relevant even when $\frac{h}{R}\ll 1$.

Taking the square root of both sides in Equation 25 gives

$$\frac{\mathrm{d}\tau}{\mathrm{d}t}=\sqrt{1-\left(\frac{R_{\mathrm{S}}}{R}-\frac{R_{\mathrm{S}}h}{R^2}\right)-\left(\frac{1}{c}\frac{\mathrm{d}h}{\mathrm{d}t}\right)^2-\left(\frac{R}{c}\,\Omega\right)^2\left(1+\frac{h}{R}\right)^2\sin^2\theta}. \tag{26}$$

Since the expression under the square root in Equation 26 differs from unity only by small quantities, we define a small parameter x as

$$x=\left(\frac{R_s}{R}-\frac{R_sh}{R^2}\right)-\left(\frac{1}{c}\frac{\mathrm{d}h}{\mathrm{d}t}\right)^2-\left(\frac{R}{c}\Omega\right)^2\left(1+\frac{h}{R}\right)^2\sin^2\theta. \tag{27}$$

We will expand the expression in Equation 26 in a Taylor series around the small parameter x. It should be noted that for the Taylor expansion $\sqrt{1-x}$ to be valid, the small parameter x must be positive. We now verify this condition numerically by estimating the magnitude of each term. The leading positive contribution comes from the gravitational time dilation near Earth's surface

$$\frac{R_s}{R} \approx \frac{8.9 \times 10^{-3\,\mathrm{m}}}{6.371 \times 10^6\,\mathrm{m}} = 1.4 \times 10^{-9}. \tag{28}$$

We next estimate the sum of the magnitudes of all negative terms entering the expression of x

$$\frac{R_s h}{R^2} + \left(\frac{1}{c}\frac{\mathrm{d}h}{\mathrm{d}t}\right)^2 + \left(\frac{R}{c}\Omega\right)^2 \left(1 + \frac{h}{R}\right)^2 \sin^2\theta, \tag{29}$$

where we assume

$$h = 3.0 \times 10^4\,\mathrm{m}, \text{ (typical HAB altitude)}, \tag{30}$$
$$c = 2.99792458 \times 10^8\,\mathrm{m/s}, \text{ (the speed of light)}, \tag{31}$$
$$v_\mathrm{a} = \frac{\mathrm{d}h}{\mathrm{d}t} = 20\,\mathrm{m/s}, \text{ (typical ascent velocity)}, \tag{32}$$
$$\Omega = 7.29212 \times 10^{-5}\,\mathrm{rad/s}, \text{ (Earth's angular velocity)}, \tag{33}$$
$$\theta = 48.6085^\circ, \text{ (colatitude at West Point, NY)}. \tag{34}$$

Evaluating numerically, we find

$$\frac{R_s h}{R^2} + \left(\frac{1}{c}\frac{\mathrm{d}h}{\mathrm{d}t}\right)^2 + \left(\frac{R}{c}\Omega\right)^2 \left(1 + \frac{h}{R}\right)^2 \sin^2\theta \approx 7.9 \times 10^{-12}. \tag{35}$$

Since the positive contribution in Equation 28 is significantly larger than the total magnitude of the negative contributions in Equation 35, we conclude that $x > 0$, and the Taylor expansion of Equation 26 is valid

$$\frac{\mathrm{d}\tau}{\mathrm{d}t} \approx 1 - \frac{1}{2}x, \tag{36}$$

and explicitly

$$\frac{\mathrm{d}\tau}{\mathrm{d}t} = 1 - \frac{1}{2}\left(\frac{R_\mathrm{S}}{R} - \frac{R_\mathrm{S} h}{R^2}\right) - \frac{1}{2}\left(\frac{1}{c}\frac{\mathrm{d}h}{\mathrm{d}t}\right)^2 - \frac{1}{2}\left(\frac{R}{c}\Omega\right)^2 \left(1 + \frac{h}{R}\right)^2 \sin^2\theta. \tag{37}$$

In Equation 37, the term

$$\frac{1}{2}\left(\frac{R_\mathrm{S}}{R} - \frac{R_\mathrm{S} h}{R^2} + \left(\frac{1}{c}\frac{\mathrm{d}h}{\mathrm{d}t}\right)^2\right)$$

captures the leading-order gravitational time dilation, including both the static contribution from the gravitational potential and the dynamic correction due to vertical motion. The final term in Equation 37,

$$\frac{1}{2}\left(\frac{R}{c}\Omega\right)^2 \left(1 + \frac{h}{R}\right)^2 \sin^2\theta,$$

represents the special relativistic (SR) time dilation arising from Earth's rotation.

As previously shown in Equation 12 and Equation 13, the rotational SR term is negligible compared to the GTD term. Neglecting this contribution, the expansion for the proper time simplifies to

$$\frac{\mathrm{d}\tau}{\mathrm{d}t} = 1 - \frac{1}{2}\left(\frac{R_\mathrm{S}}{R} - \frac{R_\mathrm{S} h}{R^2} + \left(\frac{1}{c}\frac{\mathrm{d}h}{\mathrm{d}t}\right)^2\right). \tag{38}$$

The leading-order term,

$$\frac{R_\mathrm{S}}{2R},$$

corresponds to the gravitational time dilation experienced by a stationary clock on Earth's surface. Substituting numerical values:

$$\frac{R_\mathrm{S}}{2R} \approx \frac{8.9 \times 10^{-3}}{2 \times 6.371 \times 10^6} = 6.96 \times 10^{-10}. \tag{39}$$

This is the dominant contribution to the deviation from proper time experienced by an idealized clock in flat spacetime. It quantifies the slowing of time in Earth's gravitational field and is typically of order one part in a billion.

The correction due to altitude h reflects the change in gravitational potential with height and is given by

$$\frac{R_{\mathrm{S}}h}{2R^2} \approx 3.28 \times 10^{-12}. \tag{40}$$

Although nearly two orders of magnitude smaller than the leading gravitational term, this correction remains significant in high-precision timing applications. It accounts for the altitude-dependent gravitational time dilation, and becomes particularly relevant for high-altitude balloon experiments and satellite-based systems.

Finally, the kinematic contribution from vertical motion, characterized by an ascent or descent speed v, enters as a special relativistic correction

$$\left(\frac{v}{c}\right)^2 \approx 4.45 \times 10^{-15}. \tag{41}$$

This term is more than two orders of magnitude smaller than the altitude correction and nearly five orders of magnitude smaller than the leading gravitational term. For typical ascent speeds of HAB payloads (on the order of $5\,\mathrm{m/s}$), this kinematic correction is negligible. Consequently, the total special relativistic contribution can be safely omitted without compromising the accuracy of the proper time calculation.

In summary, gravitational time dilation at Earth's surface is the dominant effect. The altitude-dependent correction is smaller but still relevant in precision timing, while the kinematic effect from vertical motion is minimal and may be neglected in most near-Earth scenarios involving slowly moving HAB payloads.

Using Equation 38, the instantaneous rates of proper time relative to coordinate time are given by

$$\frac{\mathrm{d}\tau}{\mathrm{d}t} = 1 - \frac{1}{2}\left(\frac{R_{\mathrm{S}}}{R} - \frac{R_{\mathrm{S}}h}{R^2} + \left(\frac{1}{c}\frac{\mathrm{d}h}{\mathrm{d}t}\right)^2\right), \tag{42}$$

$$\frac{\mathrm{d}\tau_0}{\mathrm{d}t} = 1 - \frac{1}{2}\left(\frac{R_{\mathrm{S}}}{R}\right). \tag{43}$$

In Equation 42 and Equation 43, dt is the coordinate time element, measured by a clock stationary in a chosen inertial frame, typically far from any gravitational source, or at rest with respect to the central mass (such as Earth). In practical applications, this corresponds to the time kept by a clock fixed on the Earth's surface or synchronized with Earth-centered inertial systems like GPS. This is often referred to as "lab frame time." Conversely, $\mathrm{d}\tau$ represents the proper time element, the time experienced by a clock moving with the object, such as one onboard a high-altitude balloon or satellite. Proper time is frame-independent and invariant, hence its designation as "proper."

The ratio $\frac{d\tau}{dt}$ quantifies how quickly proper time elapses relative to coordinate time. A value less than one indicates that the moving clock ticks more slowly than the lab frame, a manifestation of time dilation. The reciprocal $\frac{dt}{d\tau}$, tells us how much coordinate time elapses for every unit of proper time, and is often the more useful quantity in applications such as GPS, where coordinate time is taken as the reference. To compute this reciprocal, we begin with the approximation

$$\frac{d\tau}{dt} \approx \varepsilon, \quad \text{with } \varepsilon \ll 1. \tag{44}$$

Taking the reciprocal and expanding to second order yields

$$\frac{\mathrm{d}t}{\mathrm{d}\tau} = \frac{1}{1-\varepsilon} \approx 1 + \varepsilon + \varepsilon^2 + \ldots, \tag{45}$$

where we used the geometric series expansion $(1-\varepsilon)^{-1} \approx 1 + \varepsilon + \varepsilon^2 + \cdots$ valid for $\varepsilon \ll 1$. This form makes explicit how small relativistic effects accumulate over time and enables precise comparisons between proper time and coordinate time in timekeeping and navigation systems.

Stopping at first order, the reciprocals of equations Equation 42 and Equation 43 are

$$\frac{\mathrm{d}t}{\mathrm{d}\tau} = 1 + \frac{1}{2}\left(\frac{R_{\mathrm{S}}}{R} - \frac{R_{\mathrm{S}}h}{R^2} + \left(\frac{1}{c}\frac{\mathrm{d}h}{\mathrm{d}t}\right)^2\right), \tag{46}$$

$$\frac{\mathrm{d}t_0}{\mathrm{d}\tau} = 1 + \frac{1}{2}\left(\frac{R_{\mathrm{S}}}{R}\right), \tag{47}$$

where $\mathrm{d}t$ is the coordinate time element at altitude h, and $\mathrm{d}t_0$ is the coordinate time element at the geoid (the reference surface).

During the experiment, we measure the coordinate time difference between two clocks: one at altitude h and one at the geoid. This difference is $\Delta t = t - t_0$. Subtracting Equation 47 from Equation 46 gives the differential rate of time between the elevated clock and the surface clock

$$\frac{\mathrm{d}t}{\mathrm{d}\tau} - \frac{\mathrm{d}t_0}{\mathrm{d}\tau} = \frac{1}{2}\left(\frac{R_S h}{R^2} - \left(\frac{1}{c}\frac{\mathrm{d}h}{\mathrm{d}t}\right)^2\right). \tag{48}$$

This differential equation expresses how the coordinate time difference Δt accumulates over the course of the flight. Given a known altitude profile $h(t)$, obtained either from direct measurement of from interpolated flight data, Equation 48 can be integrated to compute the proper time $\tau_h(t)$ experienced by the high-altitude clock. In practice, this relation was used to assess the feasibility of detecting gravitational time dilation using a chip-scale atomic clock aboard a high-altitude balloon payload.

To compute the accumulated proper time difference $\Delta t(\tau)$, we integrate the time differential from Equation 48

$$\Delta t(\tau) = \int_0^\tau \left(\frac{\mathrm{d}t}{\mathrm{d}\tau'} - \frac{\mathrm{d}t_0}{\mathrm{d}\tau'}\right)\mathrm{d}\tau' = \frac{1}{2}\int_0^\tau \left(\frac{R_S h(\tau')}{R^2} - \left(\frac{1}{c}\frac{\mathrm{d}h}{\mathrm{d}\tau'}\right)^2\right)\mathrm{d}\tau'\,. \tag{49}$$

Here, τ is the proper time recorded by the high-altitude clock, and the integral accumulates the difference in coordinate time experienced relative to the geoid clock.

Given a discretized altitude profile $h(t_i)$, where t_i is the i^{th} time step in coordinate time, we approximate the integral using a method such as the trapezoid rule

$$\Delta t(t_N) \approx \sum_{i=1}^{N} \frac{\Delta t_i}{2}\left[f(t_{i-1}) + f(t_i)\right], \tag{50}$$

where

$$f(t) = \frac{R_S h\,(t)}{R^2} - \left(\frac{1}{c}\frac{\mathrm{d}h\,(t)}{\mathrm{d}t}\right)^2, \tag{51}$$

and $\Delta t_i = t_i - t_{i-1}$. The derivative $\frac{\mathrm{d}h}{\mathrm{d}t}$ is computed numerically using finite differences

$$\frac{\mathrm{d}h}{\mathrm{d}t} \approx \frac{h(t_i) - h(t_{t_i-1})}{t_i - t_{i-1}}. \tag{52}$$

This approach enables efficient computation of $\Delta t(\tau)$ from empirical altitude data collected during flight. By comparing this theoretical prediction to observed time differences from onboard atomic clocks, the effects of gravitational time dilation can be quantitatively assessed.

III. Specific Methodology for Operation

Characterizing CSACs follows procedures similar to those used for other types of precision clocks. Below, we outline our specific methodology, which involves the use of frequency counters to evaluate CSAC performance under various conditions, as detailed in later sections.

A. *Frequency Counters*

- A frequency counter referenced to a 10 MHz reference signal was used, with the reference provided by either a second CSAC, an FS725 benchtop rubidium frequency standard, or a GPS-disciplined oscillator.
- The counter was triggered using a signal in the range of $1.4 - 2.5$ V, collecting frequency measurements at one-second intervals over extended periods (typically exceeding 24 hours) to allow calculations of the Allan deviation for averaging times up to 28,000 τ.
- Frequency data from the CSAC was exported in comma separated values (CSV) format and analyzed to extract the Allan deviation and related metrics.

This procedure forms the foundation of our CSAC characterization efforts conducted outside of HAB flights. CSACs deployed on HABs are subject to a range of external factors that may influence their performance. This will be discussed in the next section.

IV. Environmental Impacts on CSAC Performance

Commercial CSACs are typically characterized under controlled conditions, with manufacturers providing specifications for stability across defined temperature ranges to ensure reliable operations. However, these specifications often do not account for the rapid and extreme environmental changes encountered during high-altitude balloon flights. Such variations introduce several factors that can degrade clock performance, and these must be carefully quantified and mitigated to ensure reliable CSAC operation in high-altitude environments.

A. Thermal Effects on Frequency Stability

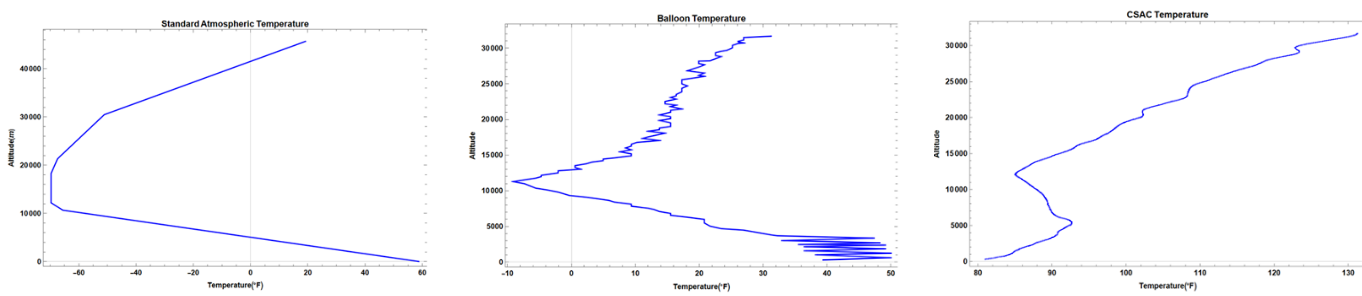

(a) Ideal temperature vs. altitude. (b) Real temperature vs. altitude. (c) Enclosure temperature vs. altitude.

FIGURE I: Temperature profiles during a high-altitude balloon flight: (a) "Textbook" atmospheric profile across the troposphere and stratosphere, (b) Ambient temperature from a sensor external to the enclosure recorded in April 2021, and (c) Internal temperature measured within the insulated CSAC container during the April 2021 flight.

Temperature fluctuations, particularly those exceeding the specified operating range, can significantly affect both the atomic physics package and the supporting electronic subsystems within a CSAC. Even within the nominal limits, rapid thermal changes can induce transient frequency shifts due to thermal gradients and differential expansion of internal components. Experimental studies have shown that the Allan deviation of CSACs can degrade by up to 30% at elevated temperatures near $50\,^{\circ}\mathrm{C}$ [4]

$$E(t) = \frac{1}{2}at^2. \tag{53}$$

In Equation 53 a represents a constant frequency drift rate. When accounting for environmental influences, particularly temperature-induced frequency variations, the model can be extended to

$$E(t) = \frac{1}{2}at^2 + \int_0^t E_i(t)\,dt + \epsilon(t). \tag{54}$$

In Equation 54 $E_i(t)$ denotes the time-varying fractional frequency offset due to environmental perturbations such as thermal fluctuations, while $\epsilon(t)$ represents random fractional frequency fluctuations, including noise and other stochastic effects [9].

Detailed analysis reveals the following temperature-dependent behavior of the Allan deviation across various averaging times (τ) in the $30\,^{\circ}\mathrm{C}$ to $50\,^{\circ}\mathrm{C}$ range

- $\tau < 10\,\mathrm{s}$: performance is dominated by short-term noise and standard fluctuations,
- $10^2\,\mathrm{s} < \tau < 10^3\,\mathrm{s}$: thermal instability introduces ramping effects, leading to mid-range degradation,
- $\tau > 10^3\,\mathrm{s}$: stability worsens significantly, with long-term drift consistent with thermal-induced shifts as modeled with Equation 54.

B. Dynamic Environmental Factors: Acceleration, Pressure, and Magnetic Fields

HAB payloads are subject to environmental stressors beyond temperature variations, including rapid acceleration, pressure fluctuations, and oscillatory motion caused by wind-induced swinging. In contrast to spaceborne satellites, where environmental conditions are relatively stable, HABs undergo rapid altitude changes that result in significant pressure variations. These fluctuations may affect CSAC's vacuum-sealed physics package and overall performance. Additionally, variations in the ambient magnetic field at high altitudes may introduce phase noise, further influencing clock stability.

C. Mitigation Strategies for Environmental Disturbances

Mitigating the effects of environmental disturbances on CSAC performance requires a combination of passive and active strategies. These strategies are essential for maintaining clock stability under the highly dynamic conditions encountered during high-altitude balloon flights.

Passive mitigation involves shielding the CSAC from environmental fluctuations as much as possible. In our implementation, thermal insulation is provided by lightweight polystyrene foam enclosure surrounding the CSAC unit. This insulation reduces the rate of heat exchange with the external environment, helping to buffer against rapid temperature drops during ascent and stratospheric float. Mechanical disturbances are mitigated through material-based damping: viscoelastic or elastomeric mounts are used to isolate the CSAC from payload structure vibrations and wind-induced swinging. These mounts reduce the mechanical coupling between the payload and the atomic clock, minimizing frequency shifts induced by acceleration and oscillatory motion.

Active compensation builds on this foundation by using environmental feedback to correct for residual disturbances. The CSAC is co-located with temperature and inertial sensors (accelerometers and gyroscopes) which continuously monitor the local environment. Post-flight, this sensor data can be used to correlate temperature excursions and dynamic motion with deviations in CSAC frequency output, allowing for retrospective frequency corrections. In future iterations, real-time compensation algorithms could be implemented on board using microcontrollers to adjust the CSAC output or to apply correction factors during the mission. These strategies would enhance CSAC resilience and stability in flight, enabling performance closer to that experienced in space borne or laboratory settings.

Future development may also explore remote operation capabilities, such as uplink commands to adjust CSAC parameters in real time, or feedback-driven control systems to actively maintain temperature and mechanical stability. These efforts will support long-duration missions and simulate space-like operating conditions with more accuracy.

V. Testing, Validation, and Future Research

A. Current and Planned Testing Procedures

Previous experiments have focused on the thermal characterization of CSACs under controlled laboratory conditions using a temperature-controlled oven. These tests have provided data on frequency stability variations at specific temperature setpoints (*e.g.*, $-44\,^{\circ}$C to $30\,^{\circ}$C). However, real-world validation is needed under the dynamic thermal conditions encountered in HAB flights, particularly during the rapid temperature transitions that occur during ascent and descent.

During a typical HAB flight, atmospheric temperature decreases steadily through the troposphere, reaching a minimum of approximately $-55\,^{\circ}$C near the tropopause at altitudes around 10-12 km. As the payload enters the stratosphere, the temperatures begin to increase gradually, reaching about $-40\,^{\circ}$C to $-20\,^{\circ}$C by 30 km altitude depending on the geographic location and the time of the year. These variations differ significantly from the steady conditions tested in the lab and must be accounted for in evaluating CSAC performance in operational environments.

τ (s)	Control	40 °C ADEV	39 °C ADEV	40 °C ADEV	44 °C ADEV
1	1.0×10^{-10}	1.2×10^{-10}	1.3×10^{-10}	1.4×10^{-10}	1.5×10^{-10}
10	3.0×10^{-11}	3.5×10^{-11}	4.0×10^{-11}	4.2×10^{-11}	4.5×10^{-11}
100	1.0×10^{-11}	1.2×10^{-11}	1.5×10^{-11}	1.6×10^{-11}	1.8×10^{-11}
1000	5.0×10^{-12}	6.0×10^{-12}	7.0×10^{-12}	8.0×10^{-12}	9.0×10^{-12}
10000	8.0×10^{-12}	9.0×10^{-12}	1.0×10^{-11}	1.1×10^{-11}	1.3×10^{-11}

TABLE I: Allan deviation values at different temperatures and averaging times.

To improve characterization, future tests will

- Extend temperature testing to a broader range, including negative temperatures encountered at high altitudes.
- Implement in-flight real-time monitoring of temperature and phase deviations.
- Introduce repeatability trials to ensure consistency across multiple flights.

B. Evaluating Holdover and Outage Performance

In practical applications, CSACs must maintain accurate timing during periods when external synchronization sources, such as GPS signals, are unavailable. This mode of operation is referred to as holdover. To evaluate CSAC performance under

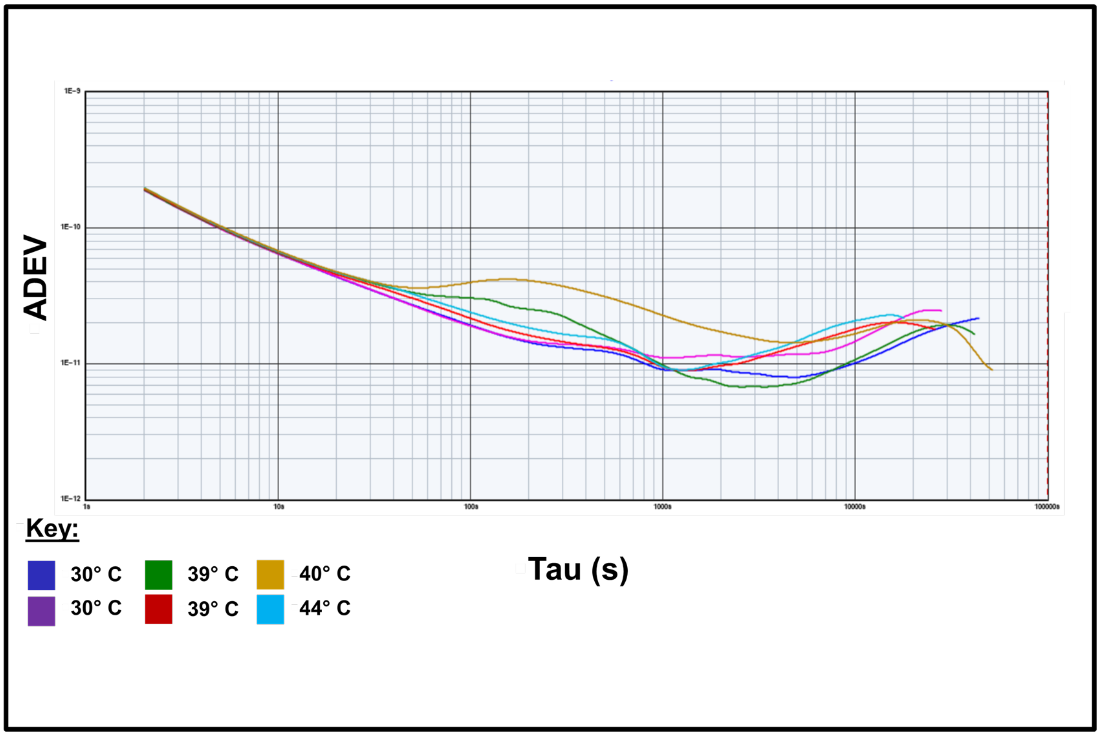

FIGURE II: Allan deviation measurements for a CSAC subjected to controlled thermal variations.

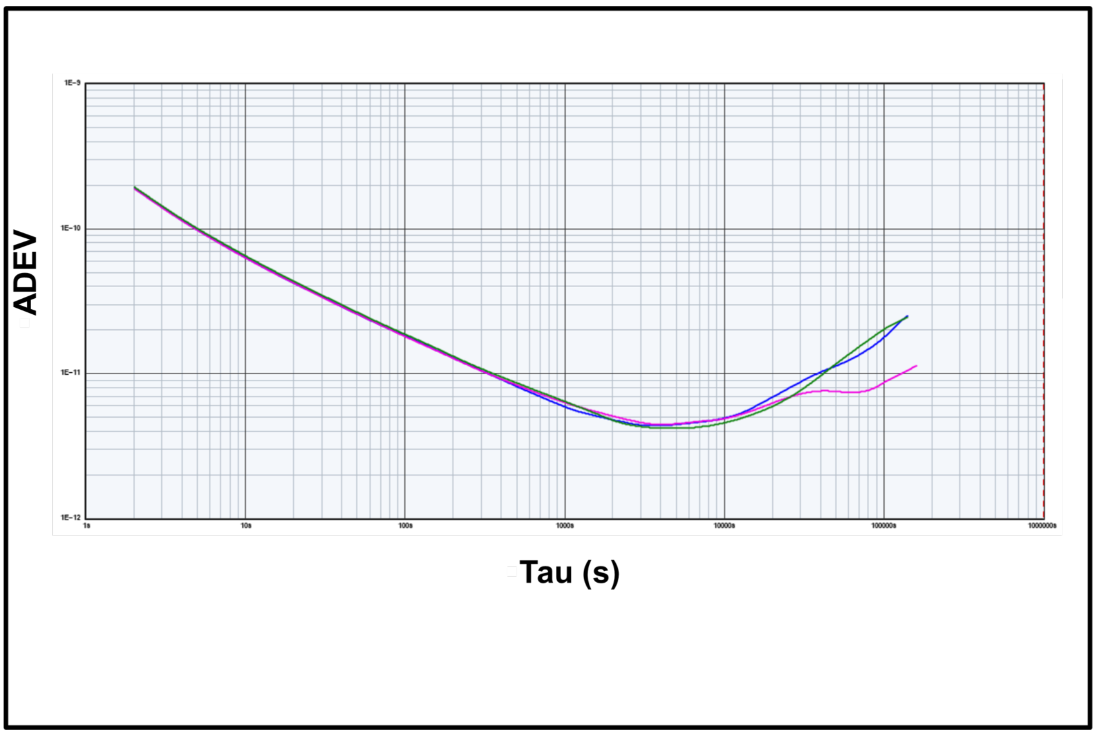

FIGURE III: Allan deviation for a CSAC at stable 25 °C.

these conditions, a controlled method involves synchronizing two CSAC units and then artificially introducing a measurement outage in one of them. By comparing the phase difference between the clocks before and after the induced outage, one can quantify the deviation due to free-running behavior. This provides a measure of the long-term frequency stability and holdover reliability of the CSAC.

C. Potential Integration with Local Positioning Systems (LPS)

Integrating CSACs with Local Positioning Systems (LPSs) offers a promising strategy for enhancing timing resilience in GPS-denied environments. LPS architectures, such as those based on ultra-wideband (UWB) signals or ground-based pseudolite transmitters, can provide localized position and time references in scenarios where GPS is unavailable or degraded.

In this context, CSACs can serve as compact, high-stability oscillators that maintain precise timing across LPS nodes. Their integration supports continuous synchronization of the system, reducing dependency on external signals and improving robustness against jamming, spoofing, or other disruptions.

The ongoing and future investigations into the integration of CSAC-LPS will inform the development of resilient timing and navigation solutions for scientific and operational applications. These efforts are especially critical for environments characterized by high dynamics, limited satellite visibility, or electromagnetic interference, where the conventional GNSS-based solution may falter.

References

[1] Microchip Technology Inc., *Low-Noise Chip-Scale Atomic Clock (LN-CSAC) SA65-LN User's Guide*, 2024th ed., Document Number: DS50003805A, Chandler, AZ, USA, available at: https://ww1.microchip.com/downloads/aemDocuments/documents/FTD/ProductDocuments/UserGuides/Low-Noise-Chip-Scale-Atomic-Clock-LN-CSAC-SA65-LN-Users-Guide-DS50003805.pdf.

[2] E. Fernández, D. Calero, and E. M. Parés, "CSAC Characterization and Its Impact on GNSS Clock Augmentation Performance," *Sensors*, vol. 2, no. 17, p. 370, 2017.

[3] L. Schement and C. Dixon, "Ground testing of a chip-scale atomic clock for maxwell cubesat flight experiment," *Proceedings of the 35th Annual Small Satellite Conference*, vol. SSC21-x-x, pp. 1–7, 2021.

[4] Microchip Technology Inc., *Chip-Scale Atomic Clock (CSAC) Performance During Rapid Temperature Change White Paper*, 2021st ed., Document Number: DS00003996A, Chandler, AZ, USA, available at: https://ww1.microchip.com/downloads/en/DeviceDoc/Chip-Scale-Atomic-Clock-CSAC-Performance-During-Rapid-Temperature-Changes-White-Paper-DS00003996A.pdf.

[5] M. S. Burns, M. D. Leveille, A. R. Dominguez, B. B. Gebhard, S. E. Huestis, J. Steele, B. Patterson, J. F. Sell, M. Serna, M. A. Gearba, R. Olesen, P. O'Shea, and J. Schiller, "Measurement of gravitational time dilation: An undergraduate research project," *American Journal of Physics*, vol. 85, no. 10, p. 757, 2017.

[6] B. Patterson, M. Serna, J. F. Sell, M. A. Gearba, R. Olesen, P. O'Shea, J. Schiller, D. Emanuel, M. S. Burns, M. D. Leveille, A. R. Dominguez, B. B. Gebhard, S. E. Huestis, and J. Steele, "An undergraduate demonstration of gravitational time dilation," *The Physics Teacher*, vol. 58, no. 4, p. 268, 2020.

[7] D. A. Howe, D. W. Allan, and J. A. Barnes, "Properties of oscillator signals and measurement methods," *Section 4: Analysis of Time Domain Data*, 2023, available at: https://tf.nist.gov/phase/Properties/four.htm.

[8] D. W. Allan, "Clock characterization tutorial," *Proceedings of the 15th Annual Precise Time and Time Interval Systems and Applications Meeting*, pp. 248–257, 1985.

[9] D. W. Allan, J. A. Barnes, F. L. Nelson, and J. A. Martin, "A technical note on the time domain characterization of frequency stability," 1981, nIST Technical Note 394, Accessed: 2025-04-13. [Online]. Available: https://tf.nist.gov/general/pdf/2220.pdf